CHAPTER 4

THE RICINUS FIELD CASE STUDY

On the basis of the interpretation of conventional surface seismic data, an exploratory well (locally referred to as the VSP well in this chapter) was drilled in the Ricinus Field, southern Alberta, Canada. The prognosis was that the VSP well would encounter the updip, raised rim of the Leduc Formation (Devonian Woodbend Group) reef complex at Ricinus Field, and would penetrate on the order of 140 m of gas pay. To the consternation of the exploration team, the well encountered only off-reef shales. The Ricinus Field had been previously defined by existing wells; some of which are shown in Figure 4.1.

As part of an investigation into the seismic images of the surrounding area, two vertical seismic profiles were conducted at the VSP well site in an effort to:

1) resolve the apparent discrepancy between the interpreted surface seismic data and the geology at the VSP well; and
2) evaluate the feasibility of whipstocking the VSP well in the direction of the reef complex.

One of the VSP surveys had a source offset of 199 m (near offset) and the other had a source offset of 1100 m (far offset). These data allowed the more confident and geologically consistent reinterpretation of the surface seismic data, and clearly indicated that whipstocking was not an economically viable option (Hinds et al., 1989a; Hinds et al., 1993c; and Hinds

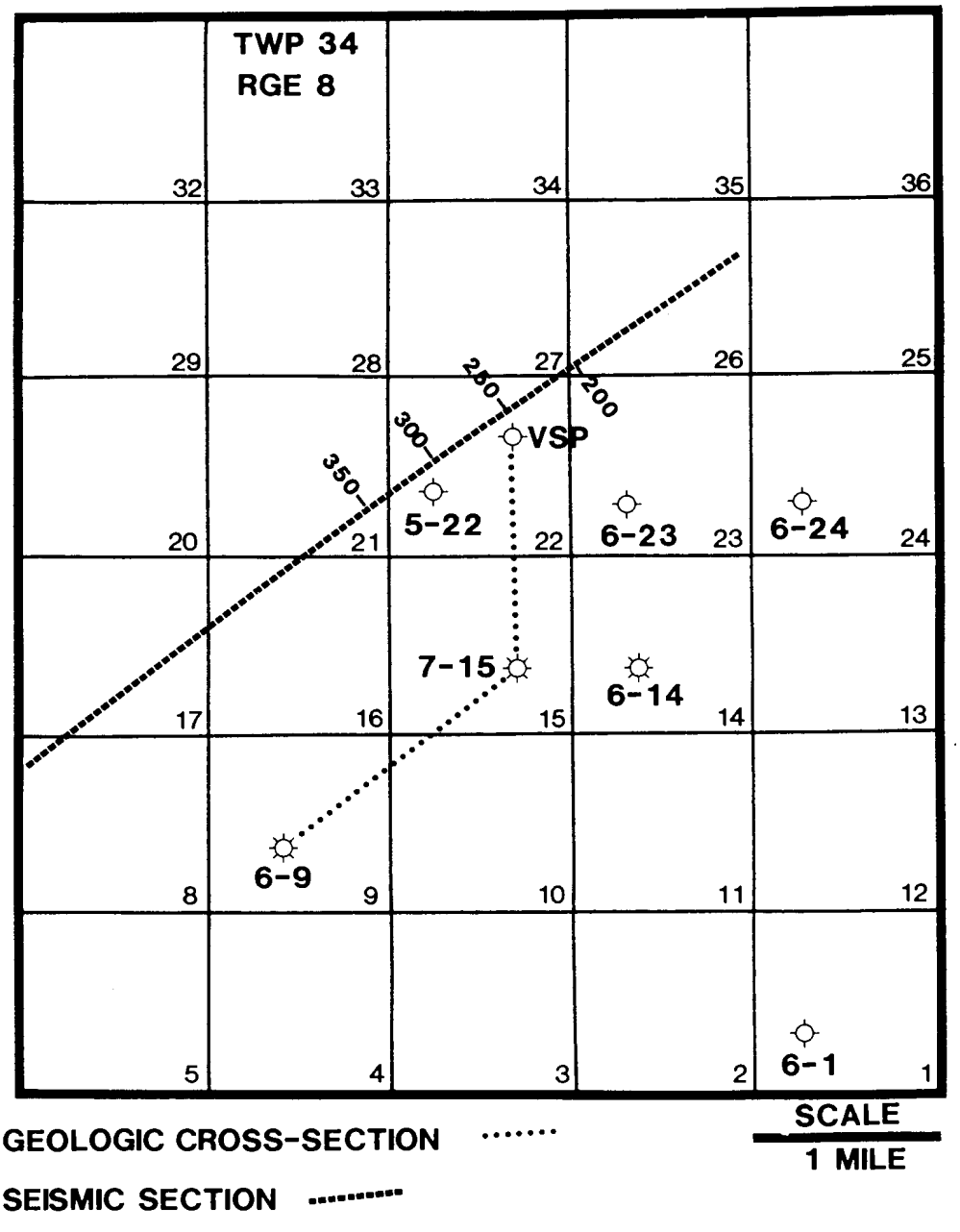

Figure 4.1 Detailed map of Ricinus study area showing the location of the wells used in the geological schematic section shown in Figures 4.2 and 4.4, the seismic data shown in Figures 4.3, 4.5 and 4.17, and locations for Leduc Formation level wells in the Ricinus Field area (from Hinds et al., 1993c; Hinds et al., 1994c).

et al., 1993c). Towards these ends, the VSP was relatively successful.

In this chapter, I present a case history that illustrates the potential for the misinterpretation of 2-D surface seismic data in the Ricinus area. This study is based on a situation where the plausible, yet ultimately inaccurate interpretation of surface seismic data led to the drilling of the VSP well. The VSP well was expected to intersect the updip edge of the Ricinus Leduc reef according to the original interpretation shown in Figure 4.2. Unfortunately it encountered only off-reef shales and was abandoned. Herein, I discuss the VSP well results, and the surface seismic and VSP data signatures at the VSP well site. The 2-D data presented were acquired prior to drilling the exploratory VSP well. The VSP survey was run in an attempt to resolve the discrepancy between the initial (pre-VSP well) interpretation of the surface seismic data and the geology at the VSP well site and to seismically image laterally away from the well towards the Southwest.

4.1 The Ricinus Field

The stratigraphy of the Ricinus Field is similar to that of the Lanaway field (Figs. 3.1A, B, and C). Similar to the situation at the Lanaway Field, the Leduc Formation at the Ricinus Field (Figs. 3.2 and 4.1), is interpreted as a large atoll which towers some 350 - 400 m (based on well 6-9-34-8 W5M) above the Cooking Lake platform and appears to exhibit a mappable peripheral raised rim and a structurally lower central lagoonal area. As at the Lanaway Field, the updip edge (northeast) of the raised rim at Ricinus is productive where it is structurally closed and effectively sealed by the inter-reef shales of the Duvernay and

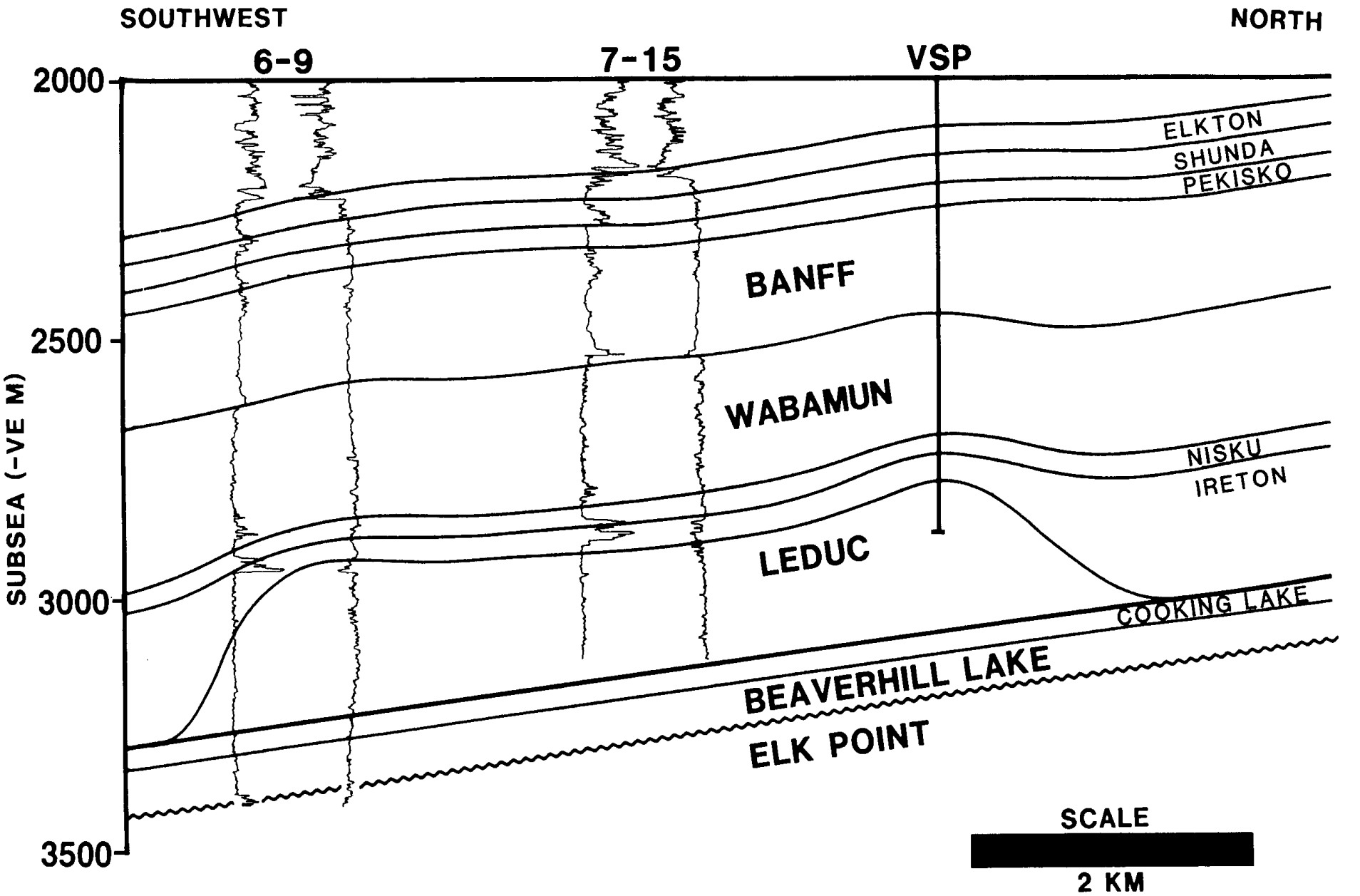

Figure 4.2 Schematic section depicting the envisioned subsurface geology at the VSP well site prior to the drilling of the VSP well. This interpretation is based on downhole data from wells 6-9-34-8 W5M and 7-15-34-8 wells and the seismic interpretation shown in Figure 4.3. The geology data from the VSP well confirmed that the seismic interpretation is incorrect. The preferred, current interpretation is shown in Figure 4.4 (from Hinds et al., 1993c; Hinds et al., 1994c).

Ireton. The schematic cross-section shown in Figure 4.2 illustrates the interpreted morphological relationships between the Leduc and the inter-reef shales of the Ireton and Duvernay in the Ricinus area (Hinds et al., 1989a, Hinds et al., 1993c; Hinds et al., 1994c).

In those areas of western Canada where the Devonian and/or overlying rock units are relatively undisturbed structurally, full Leduc reefs and inter-reef shales can usually be differentiated on seismic data. These carbonate build-ups are typically characterized by appreciable velocity pull-up (up to 25 ms), significant time-structural drape at the top of the Devonian (up to 70 ms at Ricinus in contrast to 25 ms at Lanaway), and character variations within the Woodbend Group (Anderson and Brown, 1987). Back from their steeply dipping margins, the tops of these reefs are generally manifested as high-amplitude troughs on reverse polarity seismic data (Hinds et al., 1993c).

The examples of low-relief reefs described by Anderson et al., (1989a), Anderson et al., (1989b) and Hinds et al., (1993b) are characterized by less than 10 ms of velocity pull-up and less than 20 ms of time-structural drape. Additionally, the reflections from the top of the reefs are difficult to differentiate from the inter-shale events. In those areas where extensive subsurface structural deformation has occurred, even the seismic image of the full Leduc reef may be effectively masked by the superimposed seismic signature of the structural complexities. Thrust faulting within Mesozoic strata in the general area of the Ricinus reef for example, can significantly affect the seismic signature of the Leduc reefs (Hinds et al., 1993c).

4.2 Ricinus Leduc reef

The diagrammatic cross-section incorporating wells 6-9, 7-15 and the VSP-well, shown in Figure 4.2, summarizes the geological and geophysical interpretation at the VSP well site prior to the drilling of the VSP well. This cross-section was based on the initial (pre-VSP well) interpretation of the example seismic data (Fig. 4.3), and well control available at that time.

The location and corresponding CDP numbers for one of the seismic sections used in the initial interpretation of the area (Figs. 4.3 and 4.5) are shown in Figure 4.1. The interpreted 12-fold surface seismic data displayed in Figures 4.3 and 4.5 were acquired using a source pattern consisting of five 1-kg charges spread over 60 m (at a single shotpoint). The shotpoint location interval was 120 m; the average shot depth was 9 m. The geophone groups consisted of nine in-line 14-Hz geophones over 30 m; the group interval was 30 m. 96 traces were recorded using DFS-V recording equipment and a split-spread geometry. The near offset geophone location was 30 m. The field anti-aliasing filter for the surface seismic was OUT/128 Hz. The surface seismic datum in the area was 1400 m ASL. The refraction statics replacement velocity used to reduce the surface seismic data to the seismic datum was 3350 m/s.

In the initial interpretation, the Leduc reef was interpreted to be fully developed in the area where the VSP-well was drilled. Ultimately, drilling confirmed that the VSP well site was off-reef and that this initial seismic-based interpretation is incorrect.

On the initial interpreted version of the seismic data displayed in Figure 4.3, the northern edge of the Leduc reef is located near trace 242, and full reef is mapped as present at the VSP well site at trace 259. This erroneous interpretation appears to be supported by the patterns of time-structural relief observed along the more prominent seismic events. For example, an event referred to as near-Cambrian event and the Cooking Lake event appear to be pulled up by about 15 ms immediately to the south of trace 242, and the Ireton, Wabamun, Nordegg and Blairmore events appear to drape by up to 25 ms across the interpreted northern edge of the reef. Note that the time-structure at the Blairmore and Nordegg events to the south of trace 314 in Figure 4.3, has been incorrectly attributed to thrust faulting within the Mesozoic section. The time-structure anomaly is seen as the Blairmore Coals and Nordegg events South of trace 290 being shallower in time in comparison to the same events North of trace 290 as a result of the faulting. This misinterpretation is consistent with the regional geology since the Ricinus Field is situated immediately to the east of the line demarcating the eastern limit of the Mesozoic thrust faulting of the Devonian rocks (see Fig. 5 of Moore, 1989a), and structural deformation of varying intensity is observed within the Mesozoic strata in this area.

The geologic section illustrated in Figure 4.4 shows the morphology of the Ricinus Field as interpreted after the drilling of the off-reef VSP well (Hinds et al., 1989a, Hinds et al., 1993c; Hinds et al., 1994c). This geologic section is constrained by well control and is based on the post-VSP interpretation of the example seismic line (Fig. 4.5) and the drilling information description of the geological formations intersected in the VSP borehole. Wells 6-9 and 7-15 (Fig. 4.1) were drilled into a full development of the reef and are productive; 6-9 encountered approximately 22 m of gas pay within the Leduc; and 7-15 encountered 140

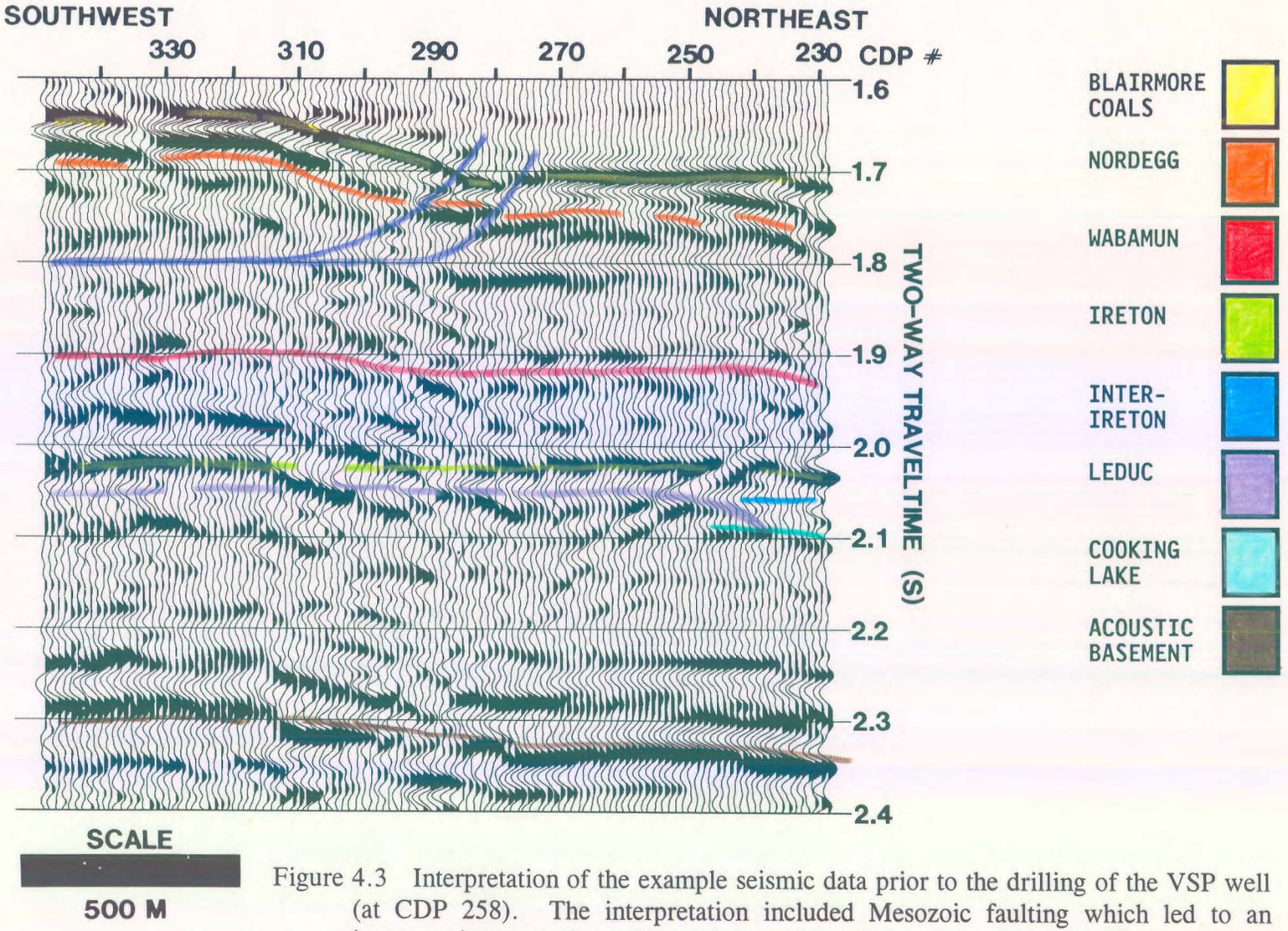

Figure 4.3 Interpretation of the example seismic data prior to the drilling of the VSP well (at CDP 258). The interpretation included Mesozoic faulting which led to an incorrect interpretation of the seismic events beneath the faulting. The preferred, current interpretation is shown in Figure 4.5. The data are normal polarity (from Hinds et al., 1993c; Hinds et al., 1994c).

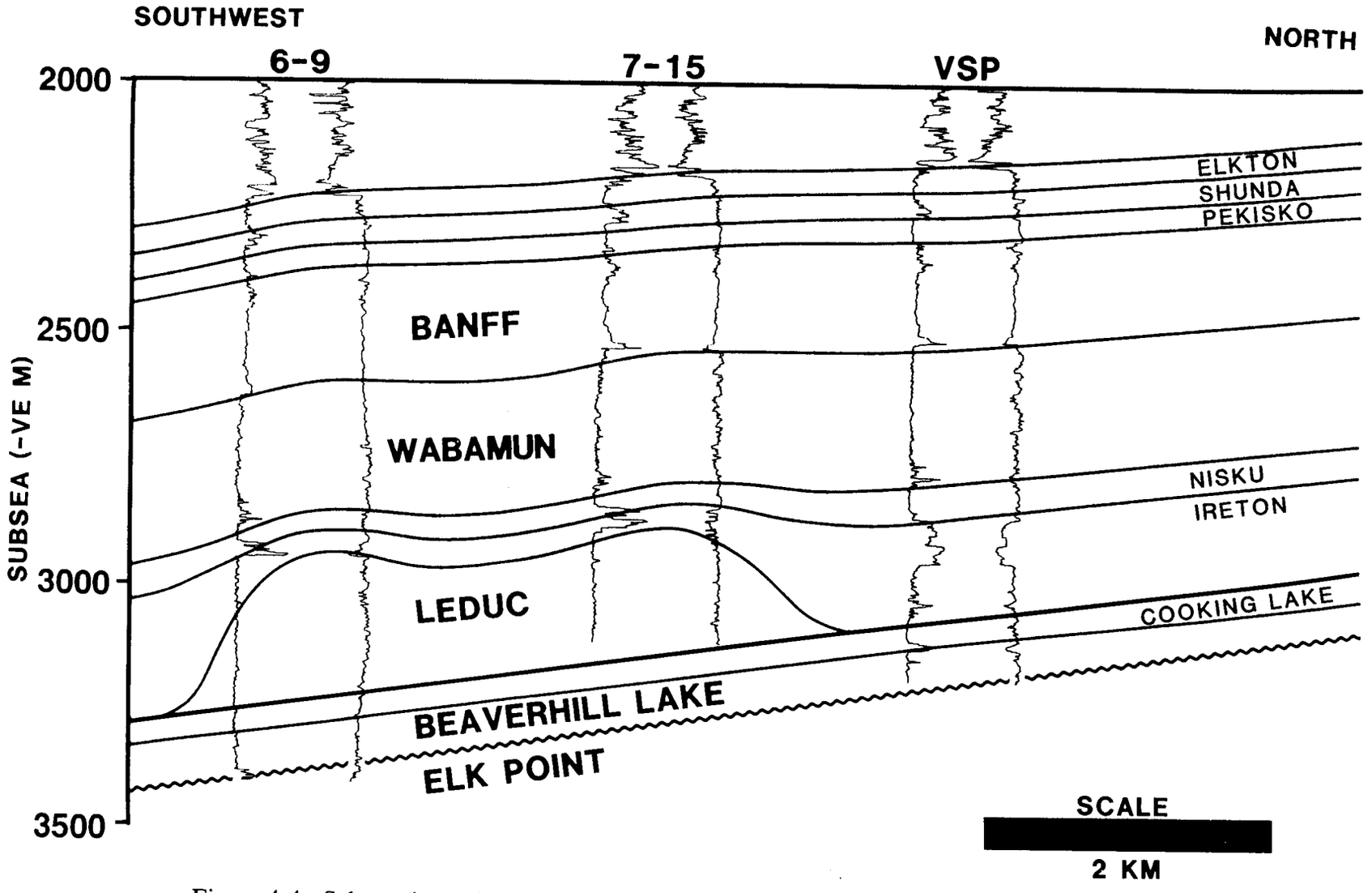

Figure 4.4 Schematic section depicting the subsurface geology at the VSP well site, and the relationships between wells 6-9 and 7-15 (locations shown in Figure 4.1) and the VSP well. The geologic section is consistent with available well log control, and the seismic interpretation displayed as Figure 4.5 (from Hinds et al., 1993c; Hinds et al., 1994c)

m of pay. Well 7-15 penetrated 250 m of Leduc reef. The VSP well (Figs. 4.1 and 4.4) is off-reef, and encountered a full section of inter-reef shale (Ireton and Duvernay; Fig. 3.1A, B and C). Well 6-9 and the VSP well encountered Cooking Lake; however 7-15 was not drilled deep enough to penetrate the Cooking Lake Formation geology.

On the post-VSP well version of the interpretation of the seismic data (Fig. 4.5), the northeastern edge of the Leduc complex is located near trace 314 and the VSP well site (trace 259) is interpreted as off-reef (Hinds et al., 1989a; Hinds et al., 1993c; Hinds et al., 1994c). This interpretation is supported by the patterns of time-structural relief observed along the more prominent seismic events. For example, the acoustic basement event appears to be pulled up by up to 40 ms to the south of trace 314; the Ireton, Wabamun, Nordegg and Blairmore events appear to drape by up to 70 ms across the interpreted northeastern edge of the reef. Note that the time-structural relief observed at the Blairmore coals and Nordegg levels to the south of trace 314, is interpreted as drape and attributed to the differential compaction of reef and off-reef sediment. In this interpretation, Mesozoic thrust faulting has not appreciably affected the rock record (Hinds et al., 1993c; Hinds et al., 1994c).

4.3 VSP data acquisition

After the analysis of the well log data and prior to abandonment, two VSP surveys were run at the VSP well site. These two VSP surveys were designed in an attempt to:

1) more accurately tie the surface seismic to the subsurface geology;

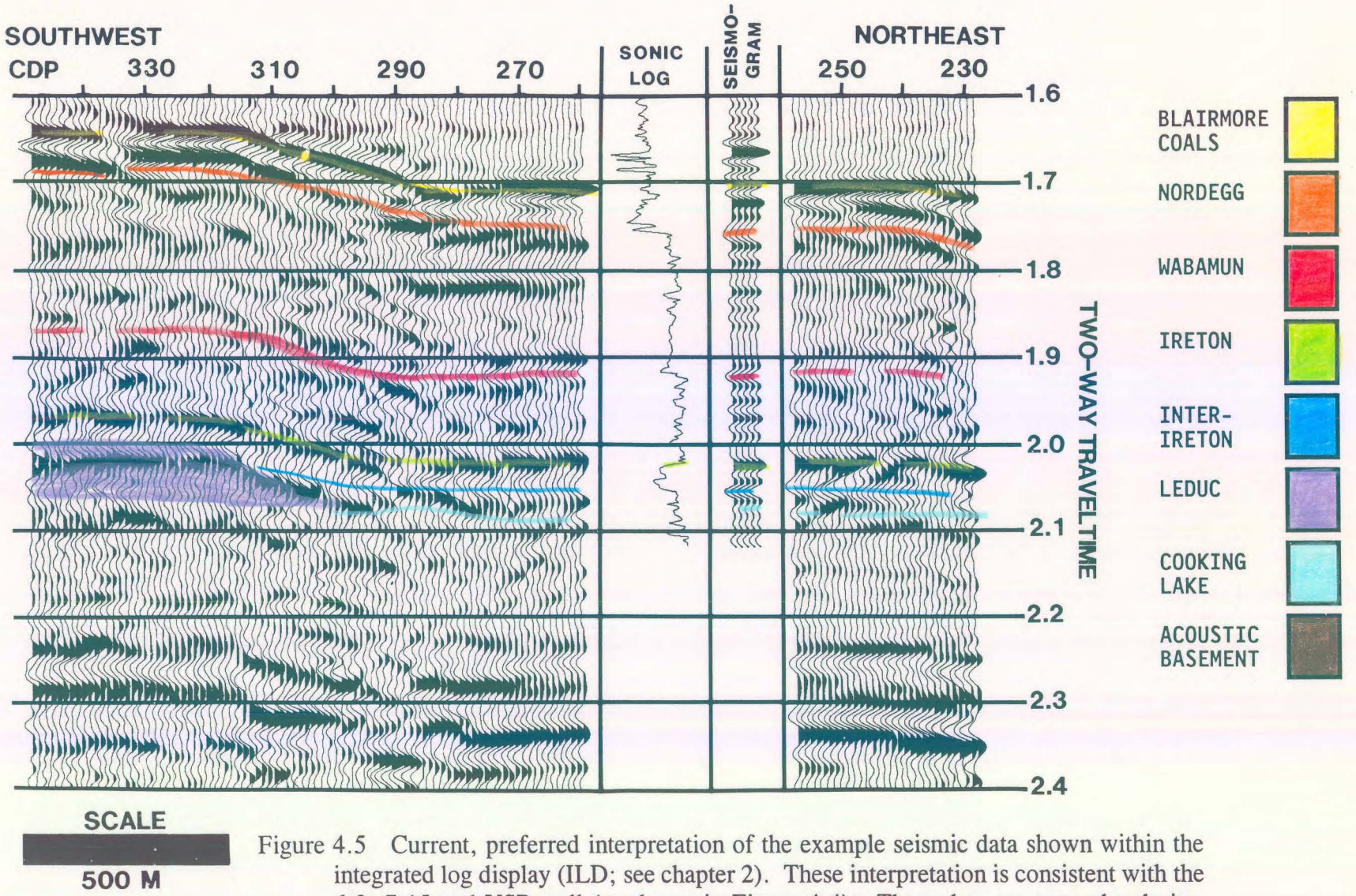

Figure 4.5 Current, preferred interpretation of the example seismic data shown within the integrated log display (ILD; see chapter 2). These interpretation is consistent with the 6-9, 7-15 and VSP well (as shown in Figure 4.4). These data are normal polarity; the display extends from 1.6 s to 2.4 s. The VSP well sonic log (displayed in time) and synthetic seismogram are inserted to display the correlations used in the interpretation (from Hinds et al., 1993c; Hinds et al., 1994c).

2) determine if the reef crest was within 500 m to the Southwest of the VSP well in the direction along the length of the example seismic line with a view to possible whipstocking; and

3) differentiate primary reflections from both surface-generated and interbed multiples.

The near offset source was 199 m from the VSP well and the far offset was 1100 m while both were on-line with respect to the surface seismic line (Fig. 4.1) and in the direction of well 5-22 to the southwest. Two Vibroseis units were operated in series at each offset position. The 16 s sweep ranged from 8 to 80 Hz, the recording length was 20 s, and the cross-correlated output was 4 s. Six to eight sweeps were summed for each geophone sonde location. The SSC 1078 VSP recording system with a sampling rate of 2 ms and a recording filter setting of OUT/OUT was used.

The total depth of the VSP well was 4528 m below KB (KB was 1317 m ASL). The source elevation of both offset source points was 1304 m ASL. Data were recorded at selected depths as the sonde was lowered down the borehole; these sonde locations were repeated during the production run. The use of these dual recording locations facilitates the detection of cable stretch or cable depth counter malfunction, and provides information regarding the gain amplification that will be required during the VSP production run. The first production VSP recording was at 4260 m below KB for the near offset VSP and 4350 m for the far offset VSP survey. During the production recording, the geophone sonde was raised at intervals of 30 m intervals until the depth of 420 m below KB. Above 420 m from the surface (KB), the depth spacing was 60 m up to the shallowest level of 180 m for the zero

offset VSP and 390 m for the far offset VSP. At each sonde location, the three component geophone tool was locked in place.

4.4 Interpretive processing of near offset (199 m) VSP data

During the processing of the near offset VSP, a series of interpretive processing panels were generated to display the following:

1) upgoing and downgoing P-wave separation;

2) deconvolution of the $\mathbf{Z_{up}(+TT)}$ data using an inverse filter calculated from the $\mathbf{Z_{down}(+TT)}$ data; and

3) inside and outside corridor stacks of $\mathbf{Z_{up}(+TT)}$ and $\mathbf{Z_{up(decon)}(+TT)}$ data.

4.4.1 Upgoing P-wave event separation

The separation of upgoing and downgoing P-waves from the **Z(FRT)** data is depicted in the wavefield separation interpretive processing panel (IPP) of Figure 4.6 (Hinds et al., 1989a; Hinds et al., 1993c; Hinds et al., 1994c).

Panel 1 displays the **Z(FRT)** data after trace normalization. In panel 2, these **Z(FRT)** data

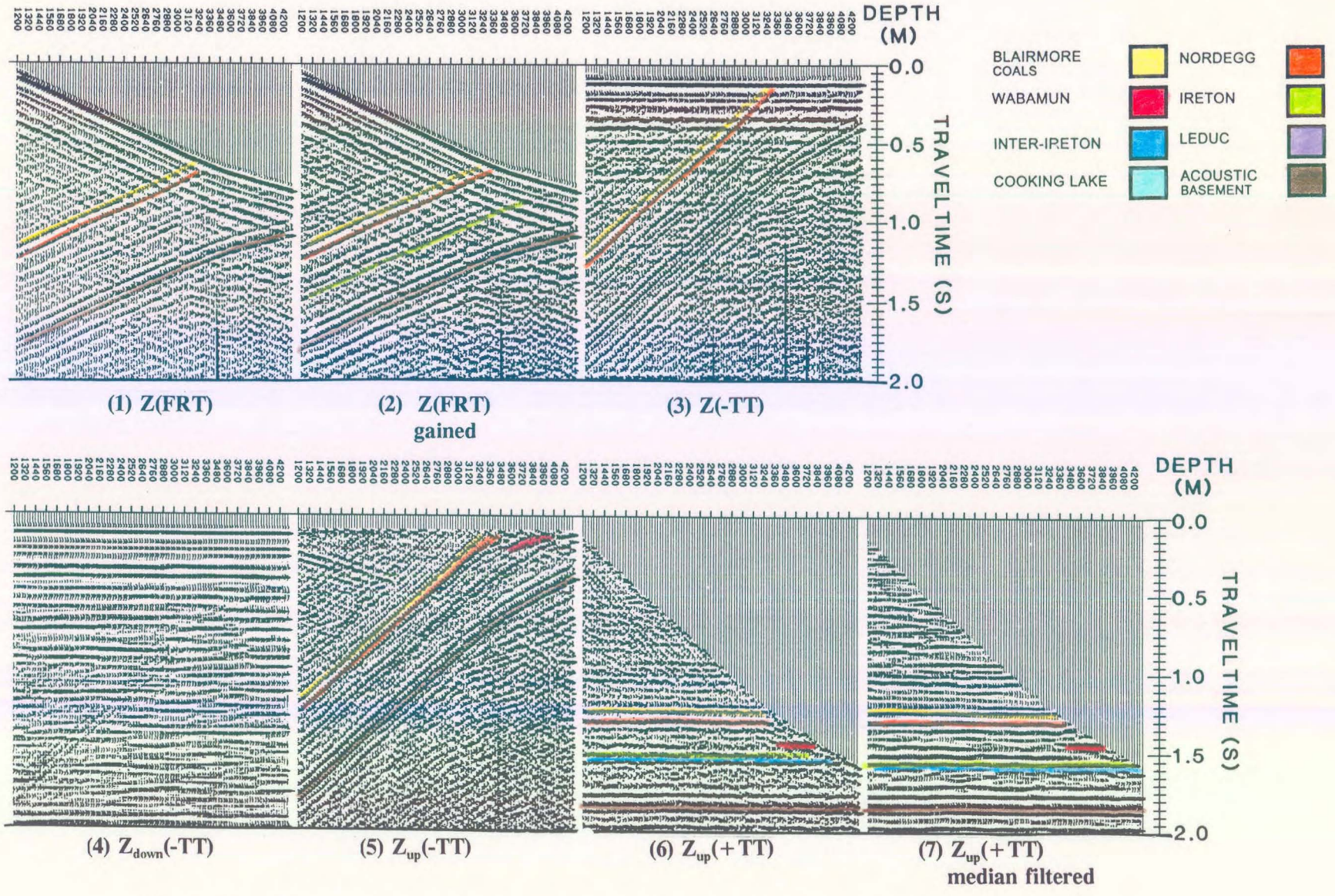

Figure 4.6 Interpretive processing panel depicting the wavefield separation of the near offset VSP data (from Hinds et al., 1989a; Hinds et al., 1993c; Hinds et al., 1994c).

have been gained to highlight several prominent primary upgoing events such as the Blairmore coals, Nordegg, Ireton and acoustic basement (crystalline Precambrian) events. Note that the upgoing event identified as the acoustic basement appears on the 4290 m trace deeper in time than the first break on that trace. Since the event does not intersect the first break curve, the event cannot be positively identified as a primary reflection as reviewed in chapter 1. The uncertainty as to the exact time and depth to crystalline basement cannot be resolved without VSP control at that depth.

The association of the downgoing surface-generated multiple (that lags the first break by approximately 0.3 s) to the upgoing events recorded below TD is bothersome when interpreting the basement reflector. On the **Z(FRT)** data in panel 2, the downgoing multiple event that intersects the deepest trace at 1.05 s coincides with the upgoing wave that begins at 1.05 s and ends on the shallowest trace at 1.65 s. The implication is that some of the events recorded below the bottom may be multiple reflections from the bottom of the borehole itself.

In panel 3 (Fig. 4.6), the **Z(-TT)** data are presented where the first breaks and downgoing P-wave multiple events are horizontally aligned. The **Z(-TT)** data in panel 3 illustrate that the downgoing wavetrain consists of the primary downgoing wavelet plus high-amplitude surface-generated multiples and less prominent possible interbed multiples. The surface-generated downgoing multiples are recognized as those horizontally aligned, post-first break arrivals that are recorded on all of the traces. As reviewed in chapter 1, if a downgoing multiple event does not extend over the entire depth range but is evident on the deeper traces only, then that multiple is interpreted to be an interbed multiple (Hinds et al., 1989a).

In the next processing step, an 11-point median filter was used to remove the upgoing P-waves. The output consisted of separated and scaled $\mathbf{Z_{down}(-TT)}$ data and is displayed in panel 4. Note that the residual upgoing wave content in the $\mathbf{Z_{down}(-TT)}$ data is minimal. This panel is one of the most important panels for interpretive processing of VSP data. If residual upgoing events remain in the $\mathbf{Z_{down}(-TT)}$ data, then that amount of residual upgoing event is subtracted out of the **Z(-TT)** data (panel 3) during wavefield separation.

The multiples that appear on all of the traces are most likely surface-generated. This is the case for multiples down to 0.45 s. Beyond that time on panel 4, surface generated and interbed multiples (as seen between 0.75 and 0.9 s) exist.

In the next step of the wavefield separation, the $\mathbf{Z_{down}(-TT)}$ data of panel 4 were subtracted from the **Z(-TT)** in panel 3 to yield the output $\mathbf{Z_{up}(-TT)}$ data shown in panel 5. The upgoing P-waves and downgoing shear waves (both primary and multiples) are shown in panel 5. The downgoing shear waves (SV) may have been generated at the bottom of the surface casing or near the surface. An example of a downgoing SV appears on the shallowest trace on panel 5 at 0.2 s (**-TT** time) and trends opposite to the upgoing events (deeper in time from left to right).

The $\mathbf{Z_{up}(+TT)}$ before and after the application of a 3-point median filter are shown in panels 6 and 7, respectively. The equalized amplitudes of the horizontally aligned upgoing waves for the Blairmore coals, Nordegg, Wabamun, Ireton, inter-Ireton, Cooking Lake, and acoustic basement events are interpreted in panel 7. It can be observed that the downgoing SV events seen in panel 5 dip more steeply in the **+TT** display; however, these events have

been effectively attenuated by the application of the median filter. As will be discussed further below, the Wabamun and Cooking Lake events have been identified only on traces deeper than the depth of the Nordegg interface due to multiple interference.

4.4.2 VSP deconvolution

On the $\mathbf{Z_{down}(-TT)}$ data, as reviewed in chapter 1, the initial downgoing pulse (except in the case of head wave contamination) is the primary downgoing P-wave; any later arriving, downgoing events are multiples (apart from downgoing shear or converted waves). Ideally, P-wave multiples can be effectively filtered using a deconvolution operator derived from an analysis of the separated downgoing P-wave wavetrain (Hardage, 1985; Hinds et al., 1989a). Deconvolution also enhances the higher frequencies within the data which allows for better vertical resolution.

The deconvolution IPP shown in Figure 4.7 (Hinds et al., 1989a; Hinds et al., 1993c; Hinds et al., 1994c) was designed to enable the monitoring of the deconvolution process of the Ricinus $\mathbf{Z_{up}}$ data. The incorporated panels reveal information (about multiples) that was difficult to determine from the wavefield separation IPP (Fig. 4.6) alone. The first two panels (Fig. 4.7) are the nonfiltered and median-filtered $\mathbf{Z_{up}(+TT)}$ data, respectively. Panel 3 contains the **Z(-TT)** data which allows an examination of the downgoing P-wave multiple pattern of the near offset data. Panels 4 and 5 contain the $\mathbf{Z_{up}(-TT)}$ and $\mathbf{Z_{up(decon)}(-TT)}$ data,

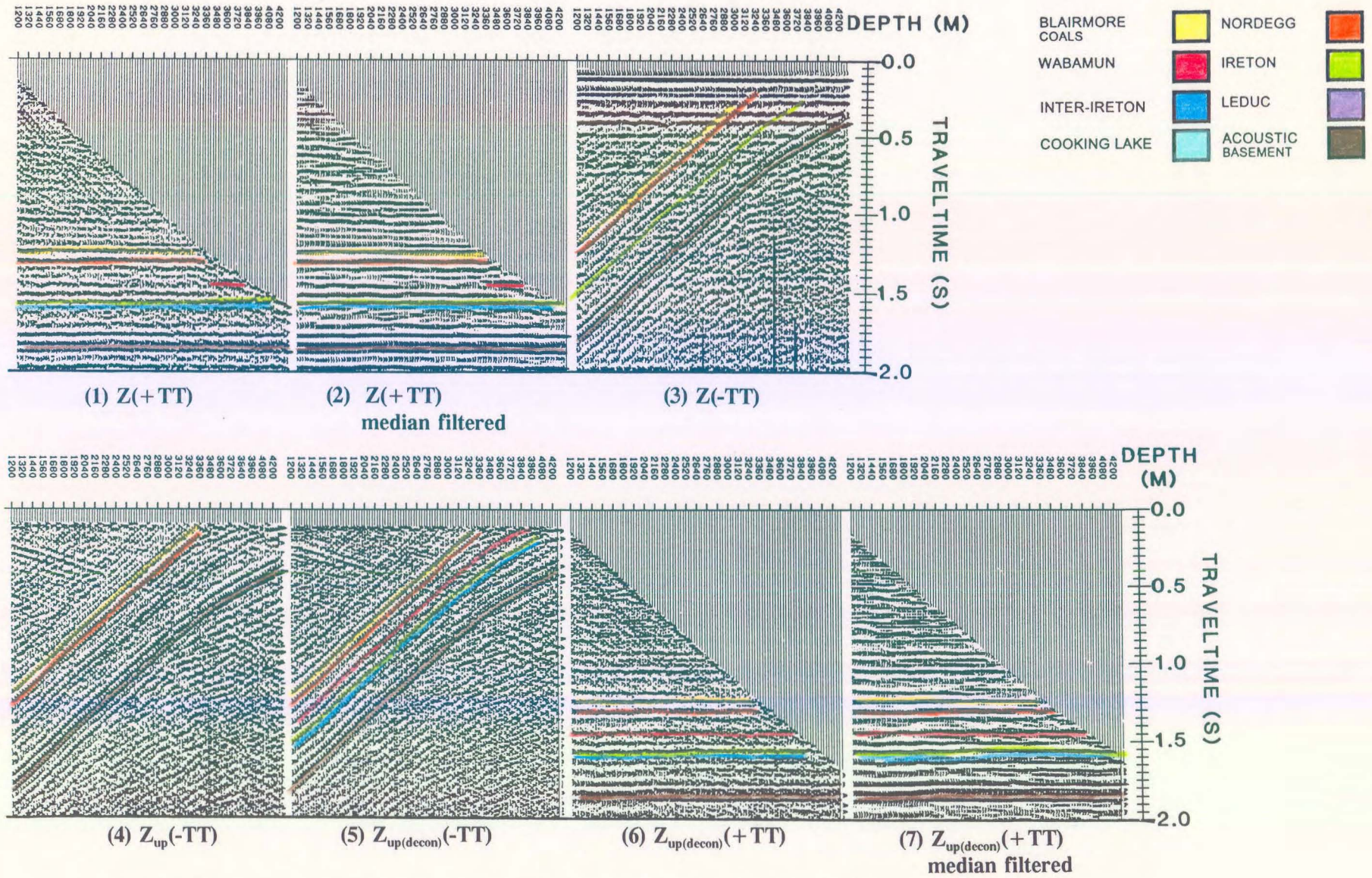

Figure 4.7 Interpretive processing panel depicting the deconvolution of the near offset VSP data (from Hinds et al., 1989a; Hinds et al., 1993c; Hinds et al., 1994c).

respectively. Both panels 4 and 5 are contaminated with downgoing shear waves. The downgoing SV events can be recognized by the observation that the events increase in traveltime with increasing depth and penetrate the upgoing events that decrease in traveltime with increasing depth. A comparison of these panels illustrates that the deconvolution process has enhanced the higher frequencies contained in the upgoing waves and preserved the primary reflections yet has not raised the noise content of the data.

The last two panels (6 and 7) contain the nonfiltered and median-filtered $\mathbf{Z_{up(decon)}(+TT)}$ data, respectively. A comparison of panels 2 and 7 (Fig. 4.7), elucidates the effect of the Blairmore coals and Nordegg multiples on the continuity of primary reflections. Multiple contamination is most noticeable for the Wabamun and Cooking Lake reflection events. On the $\mathbf{Z_{up}(+TT)}$ data in panel 2, the Wabamun is relatively unaffected on traces that are recorded below the Nordegg depth of 3466 m (-2151 m ASL). The upgoing multiple reflection from the Nordegg will not be detected on traces deeper than the bottom-generating layer of the multiple (the Nordegg) because, by definition, the multiple is an upgoing wave, not downgoing. Examination of panel 3 reveals that a series of possible surface-generated multiples exist (a series of events parallel to the first break primary (**-TT**) that are delayed in time). The multiple contamination may persist for 0.4 s or more. It is likely that both surface-generated and interbed multiples may be contaminating the $\mathbf{Z_{up}(+TT)}$ data at the Wabamun event time level. On traces recorded at depths shallower than 3466 m, the multiple events generated at the Nordegg Formation interface destructively interferes with the Wabamun event.

A trough interpreted to be the Cooking Lake event is just below the inter-Ireton trough in

panel 2 ($\mathbf{Z_{up}(+TT)}$ data) on the traces from depth 3466 m to the bottom of the borehole. The interpretation of the Cooking Lake event (Hinds et al., 1993c) is supported by the sonic log/synthetic seismogram Cooking Lake correlation to the surface seismic (ILD) shown in Figure 4.5 (the sonic log was integrated to create a synthetic seismogram and corrected using the VSP first break times). What effect does deconvolution have on the Wabamun and Cooking Lake events?

An investigation of the effect that deconvolution has on the Wabamun and Cooking Lake events shows that the Wabamun event is now laterally continuous on the $\mathbf{Z_{up(decon)}(+TT)}$ data in panel 7 (Fig. 4.7) and can be correlated on all depth traces as a result of the deconvolution. The Cooking Lake event (trough) can also now be confidently interpreted since the event is now a recognizable event across the entire $\mathbf{Z_{up(decon)}(+TT)}$ data.

The multiple contamination is interpreted to be minimal in the zone of interest around the Ireton event. The inter-Ireton is continuous and does not exhibit significant structure either before or after the VSP deconvolution. It is the inter-Ireton event that will rise and/or truncate against any Ricinus reef edge and is therefore regarded as a vital key to the interpretation success of the VSP surveys (Hinds et al., 1993c).

4.4.3 Inside and outside corridor stacks

Inside and outside corridor stacks (Hinds et al., 1989a) and associated displays for the nondeconvolved $\mathbf{Z_{up}(+TT)}$ data are presented in Figure 4.8. A comparison of the $\mathbf{Z_{up}(+TT)}$ outside and inside corridor stacks (panels 3 and 4, respectively) illustrates the utility of these displays. For example, the multiple interference generated by the Blairmore coals or Nordegg interbed multiple can be interpreted on the inside corridor stack but is not seen on the outside corridor stack. On the $\mathbf{Z_{up}(+TT)}$ data outside corridor stack in panel 3, the Wabamun trough dominates (at 1.85 s); however the $\mathbf{Z_{up}(+TT)}$ data inside corridor stack at the same time window shows no semblance of a Wabamun event. This is due to multiple interference that has destructively interfered with the Wabamun event on the depth traces shallower than the Nordegg primary (the same depth trace range that the Nordegg multiples must exist on; Hinds et al., 1989a; Hinds et al., 1993c; Hinds et al., 1994c).

On the unmuted input data for the corridor stack displays (Figure 4.8, panels 1 and 6), it can be noted that the Cooking Lake event exists as a trough beneath the inter-Ireton event (trough). The event is so weak without the deconvolution that even the outside corridor stack does not show the Cooking Lake trough. This indicates the reason for displaying the unmuted input data in the corridor stack IPP during interpretive processing (Hinds et al., 1989a). In order to interpret the outside corridor stack, it must be borne in mind what went into the stack (where the corridor mute line is).

On the $\mathbf{Z_{up(decon)}(+TT)}$ data corridor stack panels of Figure 4.9, the Wabamun and Cooking Lake events can now be reliably interpreted.

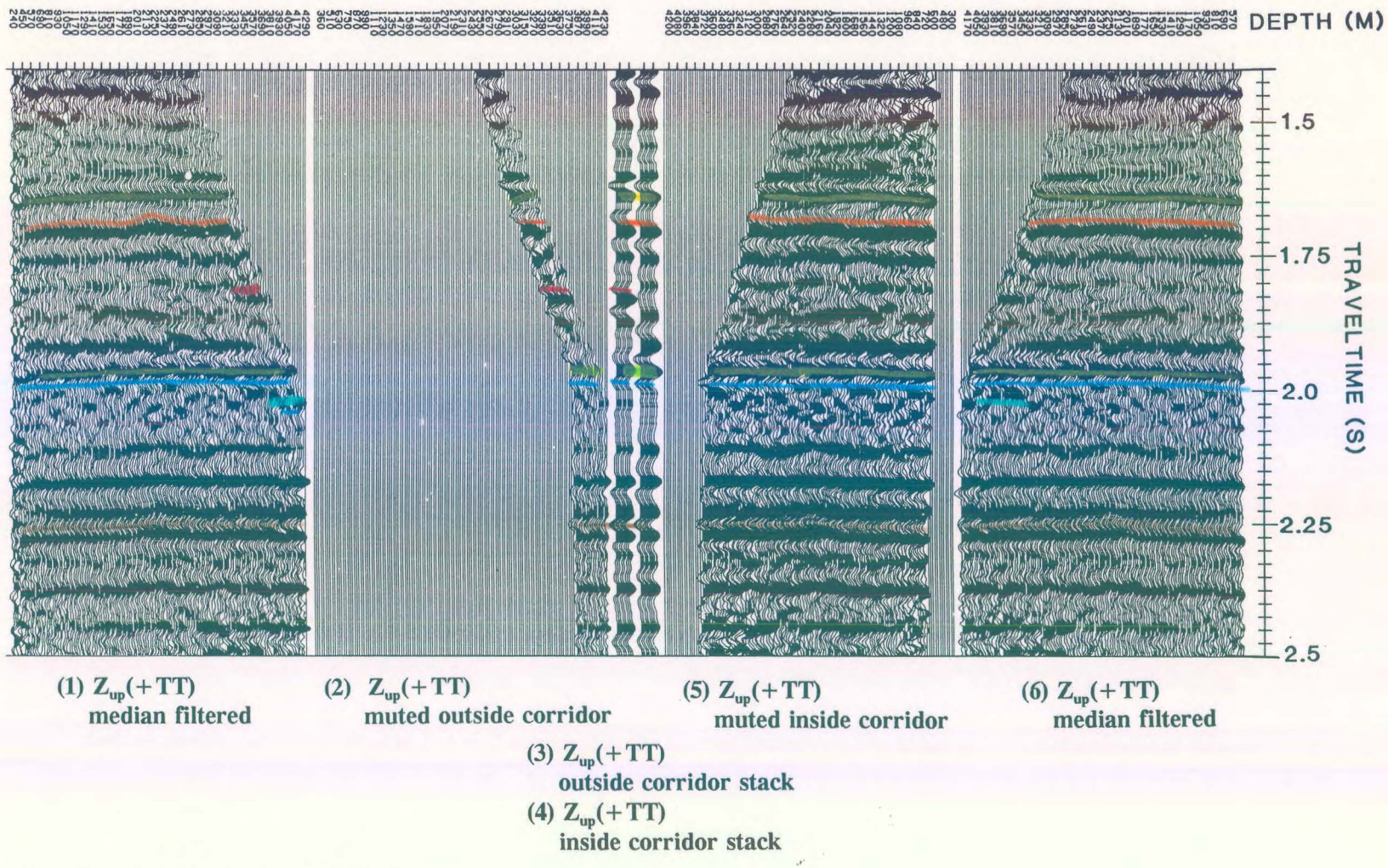

Figure 4.8 Interpretive processing panel illustrating the utility of the nondeconvolved inside and outside corridor stacks for the Ricinus near offset $Z_{up}(+TT)$ data (from Hinds et al., 1989a; Hinds et al., 1993c; Hinds et al., 1994c).

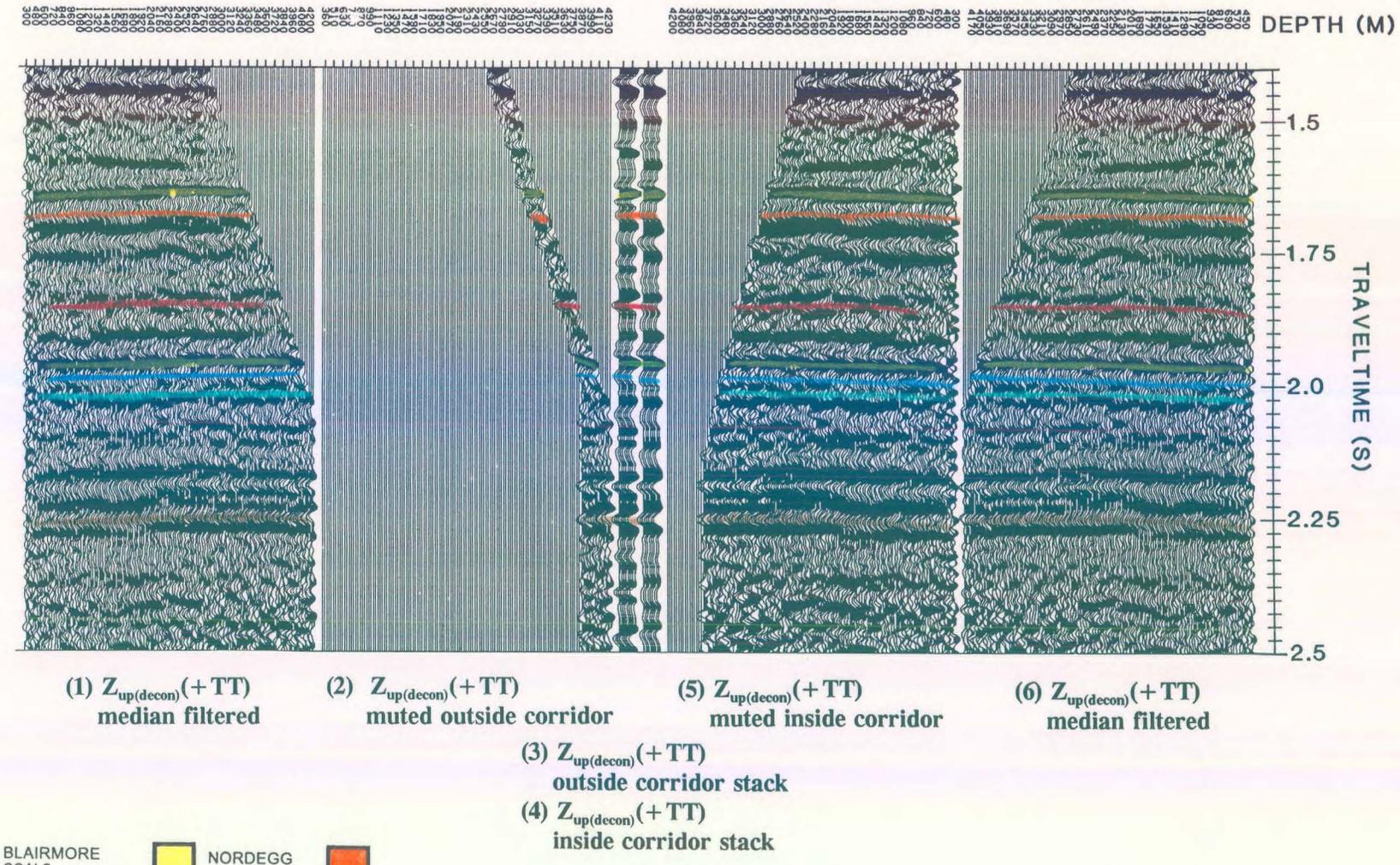

Figure 4.9 Interpretive processing panel illustrating the utility of the deconvolved inside and outside corridor stacks for the Ricinus near offset $Z_{up(decon)}(+TT)$ data (from Hinds et al., 1989a; Hinds et al., 1993c; Hinds et al., 1994c).

If deconvolution is successful, the $\mathbf{Z_{up(decon)}(+TT)}$ outside and inside corridor stacks (panels 3 and 4; Fig. 4.9) should be similar. The inside and outside deconvolved corridor stacks show that the surface generated multiples have been substantially attenuated by the VSP deconvolution process; however there is enough difference (as in the zone immediately below the Nordegg event at about 1.75 to 1.8 s) between the events of the two stacks to predict that any possible interbed multiples have been simply attenuated but not totally removed.

The deconvolved data and the corridor stacks show that the Wabamun and Cooking Lake primaries are flat lying continuous upgoing primary events across the entire VSP panel once the effect of multiple contamination is minimized. At this point the surface seismic can be reinterpreted at the well location by making use of the VSP results.

4.5 Interpretive processing of the far offset (1100 m) VSP data

On the far offset VSP data, the vertical (**Z**), and both horizontal (**X** and **Y**) axis contain nonpartitioned elements of the upgoing and downgoing P- and SV-wavefields. Examination of the IPPs to follow will reveal that the partitioning of the wavefields (both up- and downgoing P and SV events) has significant implications with respect to interpretation. In chapter 2, the Ricinus far offset data was utilized as an example of a problematic VSP data for interpretive processing. It was these data that showed how interpretive processing aided in the searching out of the origins of the problematic "noise" wavefields within the example far offset data. In this section, the interpretive processing will be shown in more detail. The reader is referred to chapter 2 with regards to the difference in runstream approaches.

As demonstrated in panels 5 and 6 of the near offset wavefield separation IPP (Fig. 4.6), a downgoing SV wave (trending in the opposite direction to the upgoing waves in panel 5) is noticeable. Normally, downgoing and upgoing shear waves are not seen on near offset data. The near offset surveys usually contain events resulting from near-vertical incidence reflections. From Zoeppritz equations, the partitioning of downgoing P waves into up- and downgoing SV waves should be minimal under conditions of near-vertical incidence reflections. It can therefore be expected that shear wave contamination will be readily noticeable on the far offset data. The runstreams used for the partitioning of the wavefields presented below will play an important role in isolating the upgoing P wave events from downgoing P wave events and up- and downgoing SV events. As illustrated in chapter 2, interpretive processing is used to assist in the modification of the processing runstreams.

Far offset IPPs have been designed to control the quality of execution of the following procedures:

1) hodogram-based rotation of the **X**, **Y**, and **Z** data (based on windowed data enveloping the P-wave first arrival; DiSiena et al., 1984, Hinds et al., 1989a);

2) time-variant model-based rotations applied to the $\mathbf{HMAX_{up}(FRT)}$ and $\mathbf{Z_{up}(FRT)}$ data in response to interpretive processing results as highlighted in chapter 2 (within the section "problematic far offset interpretive processing"); and

3) the VSP-CDP mapping of the data (Dillon and Thomson, 1984).

4.5.1 Hodogram-based rotation

The **X(FRT)**, **Y(FRT)**, and **Z(FRT)** data for the far offset VSP are displayed in Figure 4.10 as panels 1, 2, and 3, respectively. The **X(FRT)** and **Y(FRT)** data contain both P and SV downgoing waves plus recognizable upgoing SV events. These upgoing SV events can be seen on both panels 1 and 2 originating at depth levels 2790 down to the deepest traces (coloured purple in panels 1 and 2). More upgoing SV events may exist originating on the shallower traces but are overpowered in amplitude by the downgoing mode-converted SV events. The **HMAX(FRT)** data in panel 5 shows a clear definition of the up- and downgoing SV events. These events (coloured pink in panels 5 and 6) slope differently to the upgoing P wave events of the **Z(FRT)** data seen on panel 3.

The partitioned downgoing primary P waves (first breaks wavelet) are consistent on both the **X(FRT)** and **Y(FRT)** data in panels 1 and 2 on traces recorded in the upper two-thirds of the borehole which may indicate that the tool was rotating on the deeper depth traces (indicated by the first breaks becoming inconsistent on a single panel). In panel 3, the **Z(FRT)** data first breaks are phase consistent.

The hodogram-based rotation of the **X(FRT)** and **Y(FRT)** data onto the **HMIN(FRT)** and **HMAX(FRT)** data is illustrated using panels 1, 2, 4 and 5, respectively. This rotation corrects for first break inconsistencies due to the rotation of the tool during the movement of the sonde up the borehole by projecting data from both of the input channels onto an axis which lies in the plane defined by the borehole and the source; namely the **HMAX(FRT)** data. **HMIN(FRT)** and **HMAX(FRT)** data are assumed to be aligned perpendicular to and

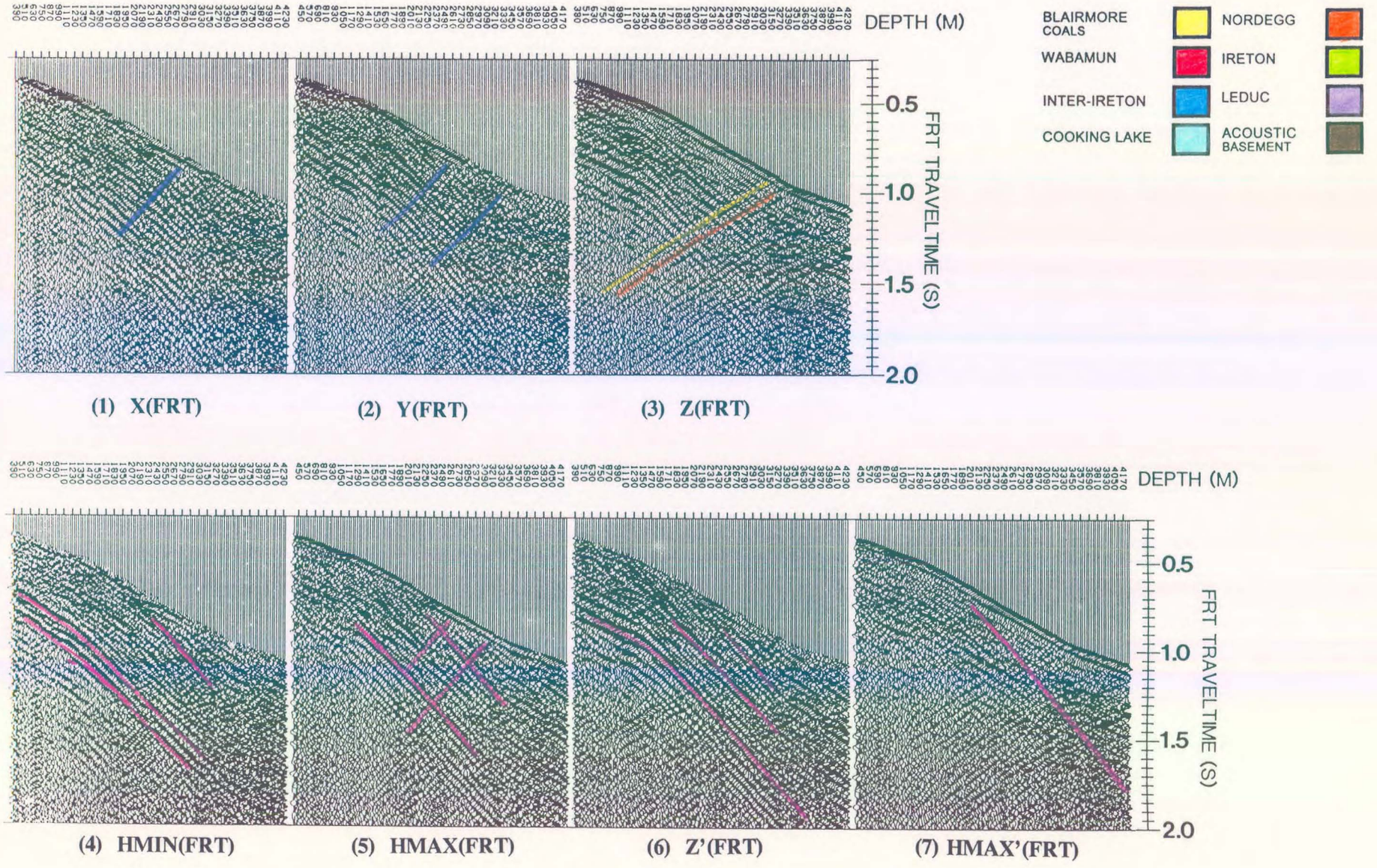

Figure 4.10 Interpretive processing panel depicting the hodogram-based rotation of the far offset Ricinus VSP data (from Hinds et al., 1989a; Hinds et al., 1993c; Hinds et al., 1994c).

in the plane formed by, the source and wellbore, respectively. Note that the **HMIN(FRT)** data (comprised of horizontally polarized shear (SH) wave events and out of the plane reflections), contains possible downgoing SV waves (coloured pink in panel 4 and appearing on the shallow traces below 0,6 s) that could originate at the casing joints or reflected downgoing waves that originate from out of the plane of the well.

The remnant of a mode-converted downgoing SV wave with components within the **HMIN(FRT)** data appears at the Nordegg and Blairmore level. The upgoing SV events from the Nordegg and Blairmore coals that were first noticed on both of the **X(FRT)** and **Y(FRT)** data are now more noticeable after redistribution onto the **HMAX(FRT)** data. These two upgoing SV events are coloured purple on panel 5. Unfortunately, the downgoing SV events on the **HMAX(FRT)** data are of equal amplitude to the downgoing P waves. The **HMAX(FRT)** data contains consistent polarized downgoing P wave first breaks as the data of the input **X(FRT)** and **Y(FRT)** channel data have been rotated into the plane containing the downgoing P wave.

The **Z'(FRT)** data in panel 6 and the **HMAX'(FRT)** data in panel 7 were obtained by rotating the **Z(FRT)** and **HMAX(FRT)** data using polarization angles estimated from a hodogram analysis of data within a window around the P-wave first arrival (DiSiena et al., 1984; Hinds et al., 1989a). This technique is designed to polarize the data so that the downgoing P-waves are effectively isolated on a single channel, **HMAX'(FRT)**.

On the **HMAX'(FRT)** data in panel 7 of Figure 4.10, the downgoing P-wave energy is

dominant. The **HMAX'(FRT)** panel contains residual downgoing shear (SV) waves (converted to SV waves at the Blairmore coal interface) and upgoing P-wave energy. This indicates that the polarization required to delineate the downgoing P-wave data onto a single panel is not adequate to separate the upgoing P-wave data entirely onto the orthogonally aligned **Z'(FRT)** data.

The **Z'(FRT)** data shown in panel 6 contains downgoing shear wave (coloured pink in panel 6) and upgoing P-wave energy that fit the assumption that the primary upgoing P-waves are orthogonal to the primary downgoing P-waves (isolated on the **HMAX'(FRT)** data). The downgoing shear wave overshadows the lower amplitude upgoing P-wave. The time-variant polarization of the data (modelled on the upgoing P-waves) should attempt to detach the contaminating up- and downgoing shear waves from the upgoing P-waves and isolate interpretable upgoing P-wave events onto a single output data panel, **Z"$_{up}$(FRT)**; however, it will be shown that this "routine-type" processing does not produce optimal results for interpretation and that a modified processing runstream is necessary (Hinds et al., 1994c).

4.5.2 Time-variant model-based rotation

The normal time-variant rotation runstream recommended in chapter 2 was used for the Ricinus far offset data and the resulting time-variant polarization IPP (Hinds et al., 1989a; Hinds et al., 1994c) is shown in Figure 2.50 and interpreted in Figure 4.11. As concluded in that example processing the **Z"$_{up}$(FRT)** data (in panel 6 of Figs. 2.50 and 4.11) contained unacceptable amounts of diffraction and mode-converted SV up- and downgoing events.

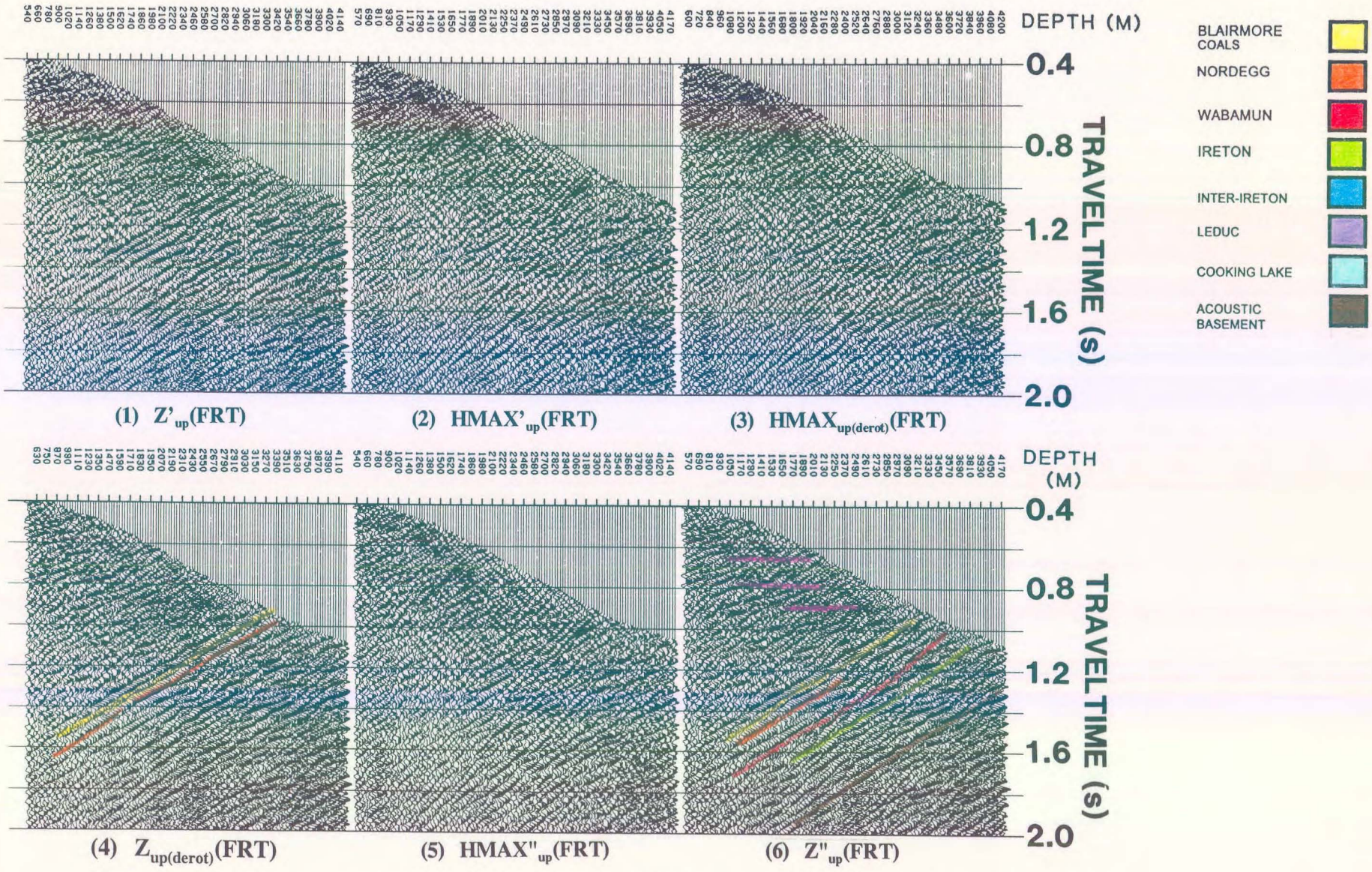

Figure 4.11 Interpretive processing panel depicting the time-variant model-based rotation of the far offset Ricinus VSP data resulting from the suggested processing runstream in chapter 2 (from Hinds et al., 1989a; Hinds et al., 1993c; Hinds et al., 1994c).

The time-variant model-based polarization runstream (as suggested in chapter 2) was changed to eliminate the second polarization rotation and to begin the runstream that eventually outputs the **Z"$_{up}$(FRT)** data by performing wavefield separation on the **Z(FRT)** and **HMAX(FRT)** data. The **HMAX'(FRT)** data displayed in Figure 4.10 were retained for the far offset deconvolution trials presented in chapter 2 and reviewed later in this chapter. The modified interpretively processed time-variant model-based polarization results are shown in Figure 4.12.

The **HMAX(FRT)** and **Z(FRT)** data (panels 1 and 2) are wavefield separated using the F-K based surgical muting (see chapter 2) to output the **HMAX$_{up}$(FRT)** and **Z$_{up}$(FRT)** data shown in panels 3 and 4, respectively. Special emphasis within the F-K mute design was taken to also attenuate the up- and downgoing SV-events from both input panels. The lack of the second hodogram-based rotation on the **Z(FRT)** and **HMAX(FRT)** input data (used in the wavefield separation) eliminated the possibility of rotation induced noise.

These data (panels 3 and 4 of Fig. 4.12) are compared to the final two panels (5 and 6) containing the time-variant model-based polarized **HMAX"$_{up}$(FRT)** and **Z"$_{up}$(FRT)** data. The emphasis is on the improvement of the quality of the upgoing P-wave events on the **Z"$_{up}$(FRT)** panel and the similar **Z"$_{up}$(FRT)** resulting from the use of the normal processing runstream (without interpretive processing) as shown in Figure 4.11. The upgoing events on panel 6 of Figure 4.12 are easily interpretable; however the same events on panels 5 and 6 of Figure 4.11 are difficult to interpret due to interfering noise. The updated **Z"$_{up}$(FRT)** does contain residual diffraction events (between 0.7 and 0.9 s and coloured pink) which manifest themselves as horizontal events.

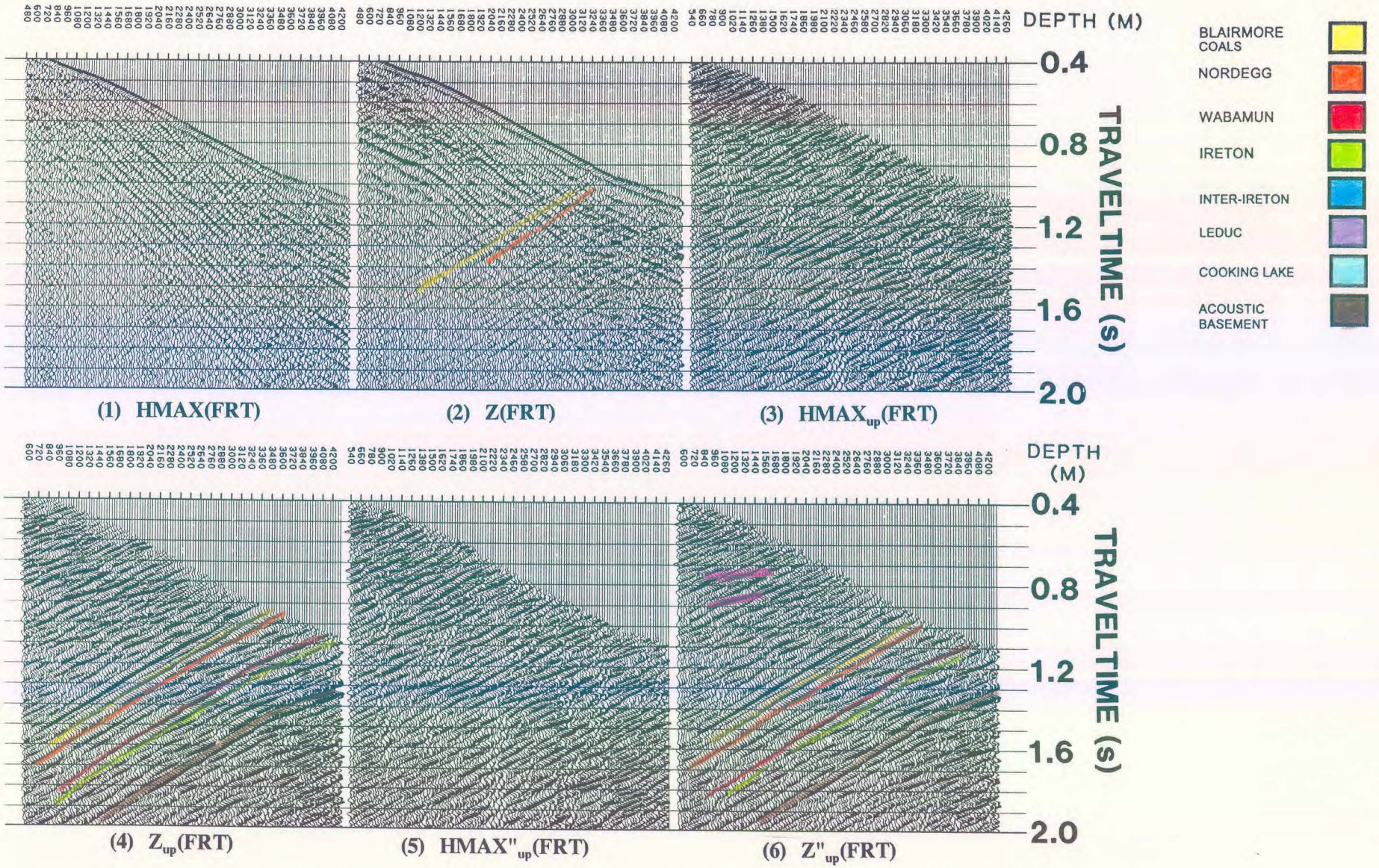

Figure 4.12 Interpretive processing panel depicting the time-variant model-based rotation of the far offset Ricinus VSP data resulting from interpretive processing (from Hinds et al., 1989a; Hinds et al., 1993c; Hinds et al., 1994c).

On the $\mathbf{Z_{up}(FRT)}$ data in panel 4 of Figure 4.12, upgoing P-waves generated by shallow reflectors are improperly aligned (due to the choice of non-time variant rotation angles). The deeper events do not suffer much misalignment because deep event raypath geometries satisfy the near-vertical incidence angle assumption better than the raypaths of shallower events. The time-variant model-based rotation corrects for this misalignment of the shallow events. The output upgoing wave displays, $\mathbf{HMAX"_{up}(FRT)}$ and $\mathbf{Z"_{up}(FRT)}$, are shown on panels 5 and 6 in Figure 4.12, respectively. Note that the shallow events display better alignment than on the $\mathbf{Z_{up}(FRT)}$ in panel 4. The rotation angle required for the Blairmore coals event on a particular trace was different to the rotation angle for deeper events (such as the acoustic basement) on the same trace. The time-variant rotation technique (Hinds et al., 1989a) generated these different rotation angles.

4.5.3 Deconvolution of the far offset data

The most realistic approximation to a far offset VSP deconvolution uses the separated polarized downgoing waves, $\mathbf{HMAX'_{down}(-TT)}$, and the separated time-variant polarized upgoing P-waves contained in the $\mathbf{Z"_{up}(FRT)}$ data, shown in panel 6 of Figure 4.12. To illustrate the deconvolution, a far offset deconvolution IPP to assist in the evaluation of the effect of far offset deconvolution on the $\mathbf{Z"_{up}}$ data (Figs. 2.56 and 4.13) has been designed. The deconvolution process involved designing the inverse wavelet for the $\mathbf{HMAX'_{down}(-TT)}$ data (panel 2 of Fig. 4.13) and subsequently applying the operator to the $\mathbf{Z"_{up}(-TT)}$ data (panel 4 of Fig. 4.13).

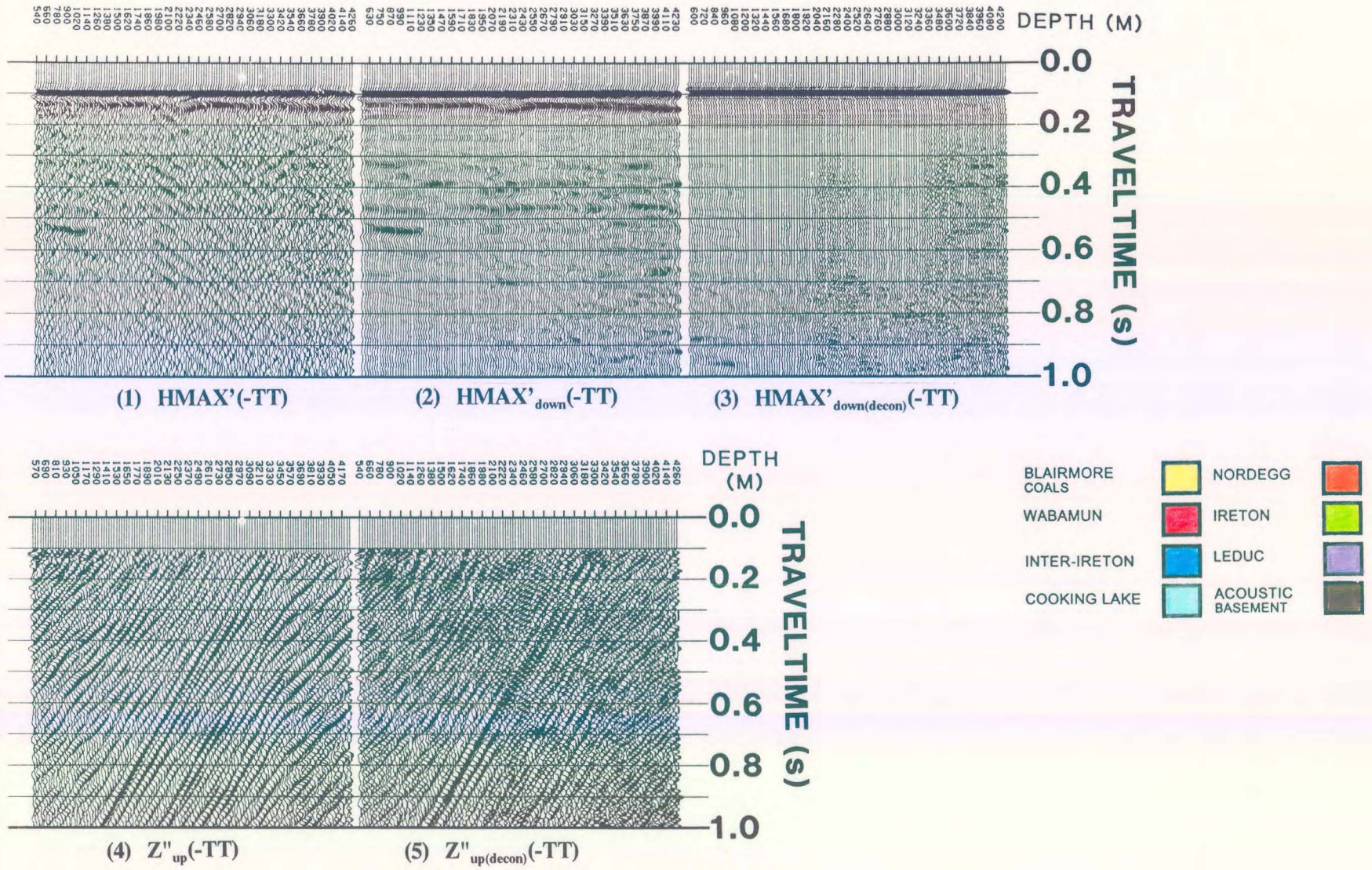

Figure 4.13 Interpretive processing panel depicting the far offset deconvolution of the Ricinus VSP data (from Hinds et al., 1993c; Hinds et al., 1994c).

The deconvolution was performed on the $\mathbf{Z"_{up}(-TT)}$ far offset data (see Figs. 2.56 and 2.57); however the process added unacceptable noise to the data. This can be seen by comparing the $\mathbf{Z"_{up}(-TT)}$ and $\mathbf{Z"_{up(decon)}(-TT)}$ data shown in panels 4 and 5 in Figure 4.13. The upgoing P-wave events have become difficult to interpret on the deconvolved data.

In the final interpretation, the non-deconvolved far offset VSP data was evaluated to contain minimal multiple contamination at the zones of interest on the $\mathbf{Z"_{up}(+TT)}$ data (on the Blairmore Coals down to the Acoustic Basement events shown in panel 6 of Fig. 4.12). For the far offset VSP data, the Blairmore or Nordegg multiples have a longer travel path to reach the Wabamun in comparison to the near offset VSP data. The Wabamun seems to be less affected on the far offset VSP data by the Blairmore coal or Nordegg multiple than on the near offset VSP data for this reason. This results in the deconvolution process for the far offset VSP data becoming a non-necessary step in the far offset processing runstream for this data.

4.5.4 VSP-CDP mapping

The $\mathbf{Z"_{up}(+TT)}$ data from panel 6 of Figure 4.12 are used for the interpretation of the off-reef markers. Two interpretation panels are used for this purpose. The first focuses on the transformation of the $\mathbf{Z"_{up}(+TT)}$ data in time (+TT) and depth into the VSP-CDP (Dillon and Thomson, 1984) domain of time (+TT) and offset distance from the well. The interpretive processing of the VSP-CDP mapping is displayed in the VSP-CDP IPP of Figure 4.14. For comparison, the VSP-CDP IPPs resulting from the normal time-variant runstream

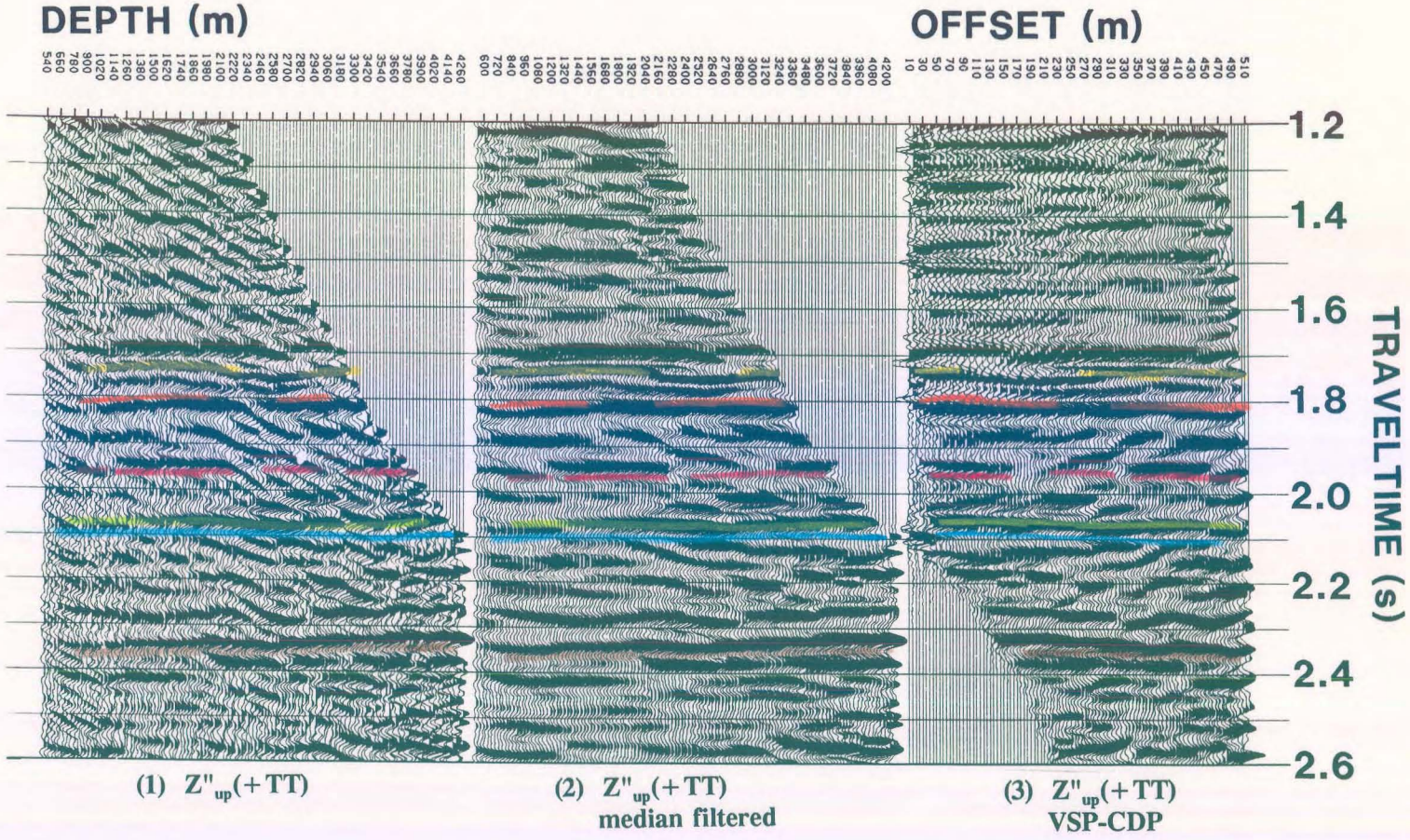

Figure 4.14 Interpretive processing panel showing VSP-CDP transformation of the non-deconvolved far offset Ricinus VSP data (from Hinds et al., 1993c; Hinds et al., 1994c).

suggested in chapter 2 and from the far offset deconvolution are presented in Figures 4.15 and 4.16, respectively. The second interpretation panel is the integrated seismic display shown in Figure 4.17 of the merged VSP-CDP display and the surface seismic data.

The $\mathbf{Z''_{up}(FRT)}$ data in panel 6 of Figure 4.12 placed in **+TT** time are shown as the first panel of the VSP-CDP IPP in Figure 4.14. A median filtered $\mathbf{Z''_{up}(+TT)}$ and the VSP-CDP mapped data (pseudo-two-way traveltime versus offset) are shown as panels 2 and 3, respectively.

The Blairmore coals, Nordegg, Wabamun, Ireton, inter-Ireton, Cooking Lake and acoustic basement markers are interpreted on these presentations. The median filtering (panel 2) as well as the VSP-CDP mapping processing (panel 3) have not appreciably distorted the interpretability of the original data ($\mathbf{Z''_{up}(+TT)}$ data in panel 1 of Fig. 4.14).

The Ireton and inter-Ireton events are interpreted to be continuous and effectively parallel indicating that only off-reef events (as opposed to reefal events) have been imaged on the far offset VSP data. In contrast, the displays in Figures 4.15 and 4.16 are difficult to interpret in comparison to the data in Figure 4.14 because of the interfering noise and deconvolution processing artifacts. Interpretive processing improved the original mode-converted up- and downgoing SV-contaminated $\mathbf{Z_{up}(FRT)}$ and $\mathbf{HMAX_{up}(FRT)}$ data sufficiently enough (as shown in the final results of Fig. 4.14) to enable a confident interpretation during each processing step.

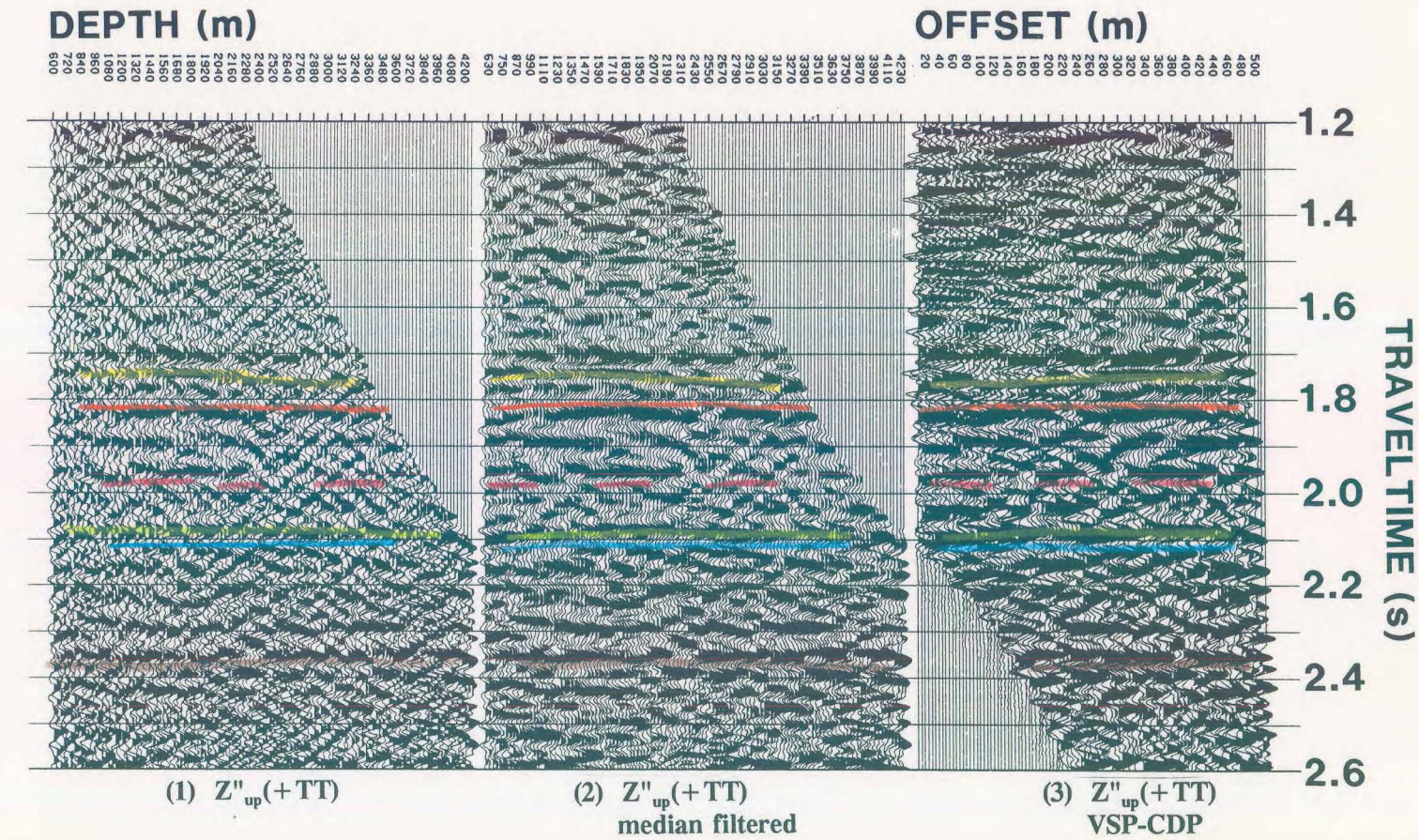

Figure 4.15 Interpretive processing panel showing the VSP-CDP transformed results for the far offset Ricinus VSP data resulting from the suggested "normal" runstream in chapter 2 (from Hinds et al., 1989a; Hinds et al., 1993c; Hinds et al., 1994c).

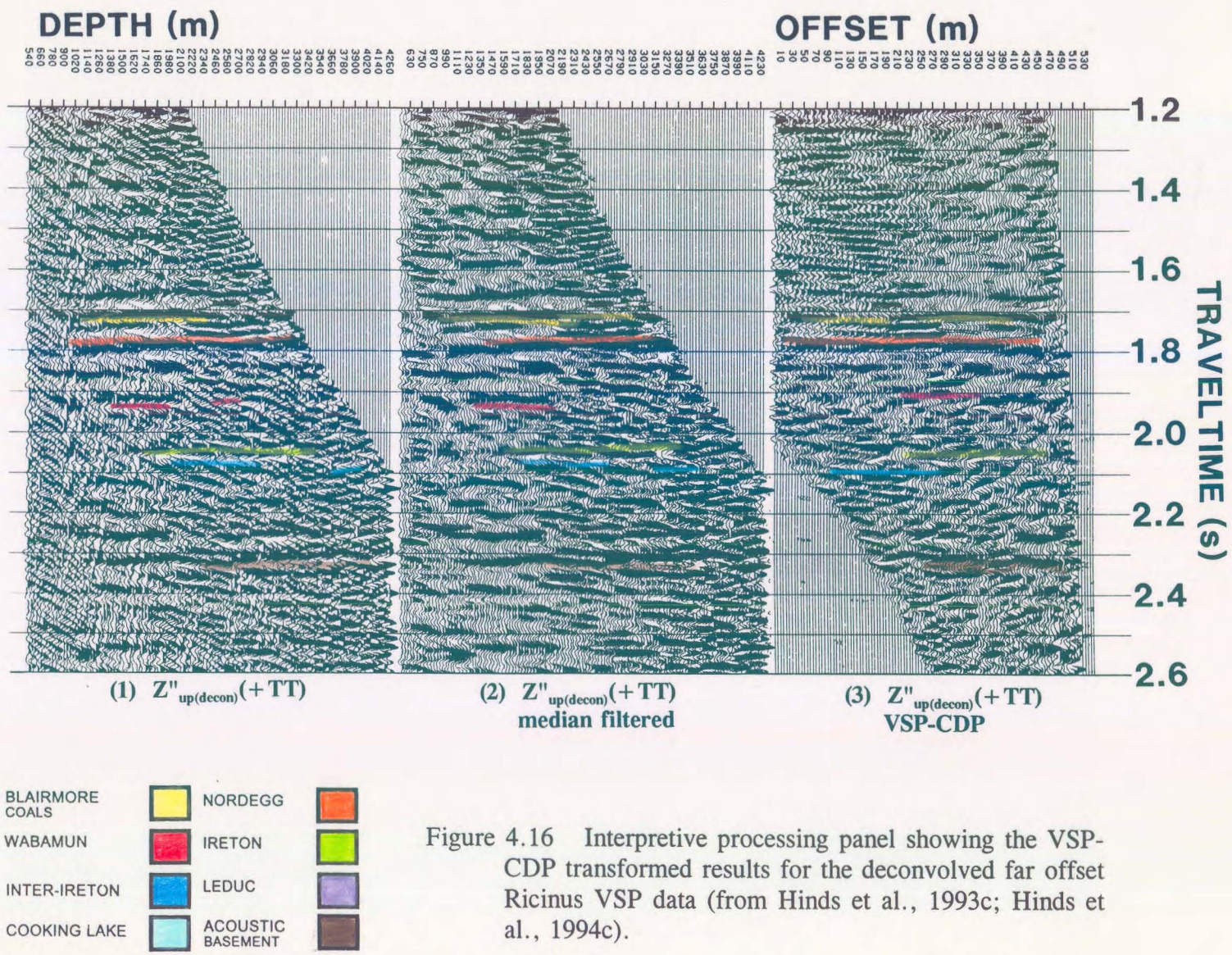

Figure 4.16 Interpretive processing panel showing the VSP-CDP transformed results for the deconvolved far offset Ricinus VSP data (from Hinds et al., 1993c; Hinds et al., 1994c).

4.6 Integrated interpretation

The integrated seismic display (ISD, see chapter 2) shows the surface seismic line merged with the VSP-CDP mapped results (panel 3 of Figure 4.14). The integrated seismic display in Figure 4.17 shows that the seismic interpretation displayed in Figure 4.3 extended the interpretation of the edge of the reef too far to the northeast, and supports the current interpretation as given in Figure 4.5.

These data also illustrate that the off-reef inter-Ireton event evident on the seismic section (Figure 4.5) extends about 500 m to the southwest. The surface seismic processing had sufficiently attenuated the SV events through the processing steps of normal moveout correction and CDP stacking. The interpretive processing enabled the desired attenuation of the SV events on the VSP data. The tie to the surface seismic up to 500 m away from the VSP well allows for the confident correlation of the inter-Ireton marker. Since only a small bundle of rays from the source to the well geophones has been affected by any Mesozoic faulting and the normal CDP summing found in surface seismic is not done in VSP processing, the coverage of the far offset VSP can be interpreted with a high level of confidence. By the processing that was applied in the rotations and the filtering which was evaluated using interpretive processing, the signal was enhanced enough to allow for an interpretation alongside the seismic data.

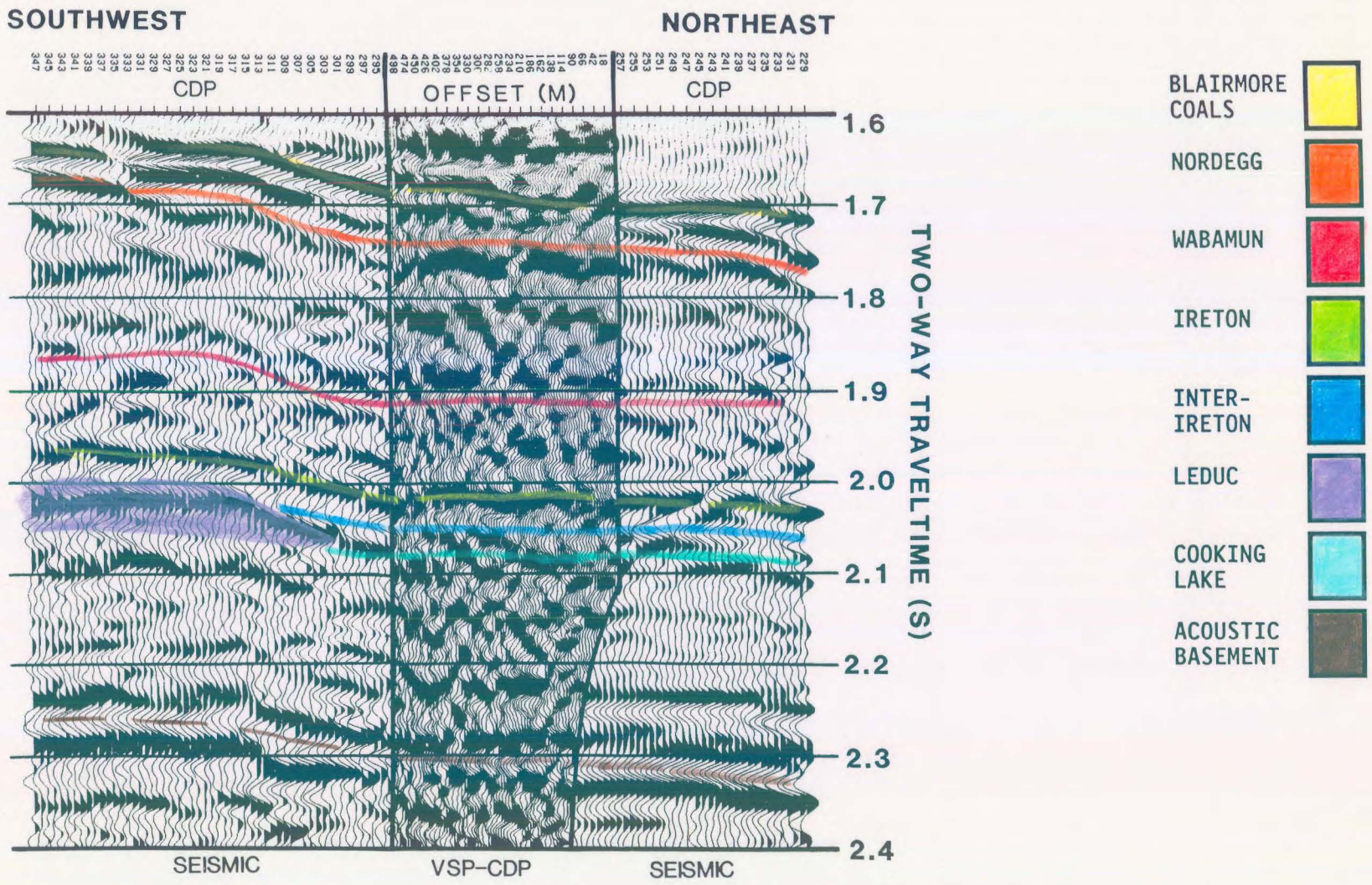

Figure 4.17 Integrated seismic display showing the VSP-CDP transformed far offset $Z''_{up}(+TT)$ data merged with the surface seismic data. These VSP data replace the surface seismic data at CDP's 258-293 (from Hinds et al., 1989a; Hinds et al., 1993c; Hinds et al., 1994c).

4.7 Interpretation discussion

The offsets for the Ricinus VSP survey were selected with the following considerations in mind:

1) If the atoll edge was in the near vicinity, then the inter-Ireton marker would terminate against the reef flank;

2) If the reef was further than 500 m (approximately half the 1100 m offset) away from the borehole or if the reef was in a different direction to the chosen offset direction, the inter-Ireton marker would be relatively flat and continuous;

3) the multiples that would affect a zero-offset seismic interpretation (migrated section) would be evident on the zero-offset VSP results; and

4) the exact geological tie with the seismic would be interpreted using the zero-offset VSP data.

The 199 m offset enabled an interpretation of the seismic signature at the well with a minimum of seismic interference from the complex Mesozoic faulting. The energy travelling down to the sonde in the borehole passes through the geological strata at near-normal incidence angles resulting in less ray bending than the CDP gathered surface seismic data. The well was in an off-reef position with the seismic interpretation being focused on the

Ireton, inter-Ireton, and Cooking Lake events rather than the Leduc event. The overlying marker that is used in isochron interpretation on the surface seismic was the Wabamun. The interpretational concern was that the Wabamun event was affected by the Blairmore coals or Nordegg multiples.

On the non-deconvolved near offset VSP data, interference with the Wabamun occurred until the geophone was below the Nordegg. The upgoing VSP events tied with the seismic section only after the VSP deconvolution was applied. The CDP stacking process within the surface seismic processing runstream enabled enough multiple attenuation to facilitate a Wabamun interpretation on the surface seismic data. The far offset VSP upgoing events did not critically require deconvolution (using the separated **HMAX'$_{down}$(-TT)** data to design the operator) and easily correlated to the surface seismic events.

The far offset VSP provided subsurface coverage for 500 m away from the VSP well site. Each trace represents approximately 6 m of subsurface coverage. The updated geological model based on the far offset VSP results is shown in Figure 4.4. In this figure, 6-9 and 7-15 are reefal; the VSP well however, is at least 500 m away from the reef edge.

The ISD in Figure 4.17 shows the seismic marker for the inter-Ireton within the range of the VSP-CDP coverage being continuous and displaying relatively little structure. Within the 500 m range away from the VSP well, the event does not terminate against the flank of the reef on the merged far offset VSP and seismic section. The Wabamun event in the far offset VSP data has not been affected appreciably by the multiples from the Blairmore coal zones due to the different geometry of the raypaths between the zero-offset VSP and the far offset

VSP. The Leduc reef event dips relatively steeply to the north of well 7-15 to the reefal platform position (Figs. 4.5 and 4.17) suggesting an abrupt edge may be present beyond 500 m southwest of the VSP well. The geological tie has been confidently interpreted from the IPP at the well location and the interpretation has been carried through to the merged far offset VSP and seismic dataset in the ISD, all using the philosophy of interpretive processing.

The mapping of the off-reef sediments enabled the final whipstock decision to be made. The decision was to abandon the well because the reef was more than 500 m away from the well location.